AGU100 ADVANCING EARTH AND SPACE SCIENCE

Geophysical Research Letters

RESEARCH LETTER
10.1029/2019GL085907

High-Resolution Ocean Wave and Wind Characteristics Determined by the ICESat-2 Land Surface Algorithm

Bradley W. Klotz[1], Amy Neuenschwander[1], and Lori A. Magruder[1]

[1]Applied Research Laboratories, University of Texas at Austin, Austin, TX, USA

Key Points:

- ICESat-2 provides high-resolution surface elevation along-track data for many unique applications
- Individual ocean waves are observed by the satellite across the region of interest and inform on important ocean characteristics
- Validation confirms and supports the significant wave height and wind speed results and highlights the ICESat-2 contribution to marine meteorology and oceanography

Supporting Information:

- Supporting Information S1

Correspondence to:
B. W. Klotz,
brad.klotz@arlut.utexas.edu

Citation:
Klotz, B. W., Neuenschwander, A., & Magruder, L. A. (2020). High-resolution ocean wave and wind characteristics determined by the ICESat-2 land surface algorithm. *Geophysical Research Letters*, *47*, e2019GL085907. https://doi.org/10.1029/2019GL085907

Received 21 OCT 2019
Accepted 19 DEC 2019
Accepted article online 23 DEC 2019

Abstract The Ice, Cloud, and land Elevation Satellite 2 (ICESat-2) is a revolutionary remote sensing tool designed to provide high-resolution height estimates of the Earth's surface. The photon counting LiDAR instrument onboard collects data over various surfaces and provides detailed information on regions where present observations are sparse or nonexistent. ICESat-2 is initiating a wave of new science, and this study examines a methodology for deriving ocean surface wave and wind characteristics. Using a modified version of the ICESat-2 land surface algorithm, individual waves are mapped along the ICESat-2 track. Significant wave features, associated ocean wind speed, and wave energy spectra are determined from the ocean data. Validation against trustworthy data sources indicate the root mean squared error of significant wave heights is 0.3 m and is 2.4 m s^{-1} for wind speed. Wave spectra are more variable but peak swell and wind seas generally agree within ±8–13% of buoy estimates.

Plain Language Summary Large changes occurring in the North and South Poles due to global warming is consistently in the news. One problem we have with really understanding the changes in those places is we do not have the right tools to study them in detail or over large areas. But now we do! There is a new satellite orbiting the Earth called ICESat-2 that is gathering information about the changes in the ice and snow heights at the poles. ICESat-2 is also able to make measurements over the oceans and land. The oceans have a wide influence on weather and climate, and ICESat-2 provides a new way for advancing ocean science. This paper talks about how ICESat-2 can see individual ocean waves and determine important information about the ocean and air above the ocean. We use this information from the waves to compare with other data and confirm that useful ocean information is available over much smaller distances with fewer assumptions about the ocean condition. The new results can lead to other studies that are related to sea ice changes in high latitudes or changes in sea level, with added potential along coastal areas around the world.

1. Introduction

Over the past few decades, advances in satellite remote sensing techniques have greatly enhanced Earth science studies. These techniques from the vantage point of space provide ongoing measurements for the lifetime of the satellite that allows both global and local studies with enhanced analysis of long-term trends of physical processes, which is not possible with aircraft or land-based remote sensing tools. In particular, ocean wave measurements and associated atmospheric parameters historically were limited to ship-based observations or locations near the coastline where data was more easily obtained with buoys or coastal radar. With the advent of satellite-based radar altimeters, synthetic aperture radars, and various radiometers, improved characteristics of the ocean surface height, wave heights, and winds became consistently attainable from space (e.g., Benveniste, 2011; Mears et al., 2015; Schultz-Stellenfleth et al., 2007; Wentz et al., 2017).

One of the typical drawbacks of space-based observations of the Earth is the horizontal resolution of the sensors. For example, observations of ocean vector winds from the Advanced Scatterometer (ASCAT, Figa-Saldaña et al., 2002) are obtained on both sides of the spacecraft with swath widths of 550 km. The large swath width allows for increased coverage of the ocean surface with higher repeat times than many satellites but typically has a resolution of ~30 km (Bourassa et al., 2019). On the other hand, the radar altimeter products from Jason-2 (Lambin et al., 2010) or Jason-3 (Desai, 2016) have an along- and cross-track resolution of 11.2 and 5.1 km, respectively. With a 10-day repeat cycle and over 300-km separation between equatorial crossings, this leaves room for large gaps in the ocean surface topography data and subsequent applications, unless merged with other data sets. Given the number of satellites that are currently active, data mergers are almost expected when designing the technical constraints of a satellite-based observing system.

Regardless of the method, scientists desire to work toward better measurements and coverage of the Earth from space. The decadal surveys that are produced by the National Research Council for the National Aeronautics and Space Administration, the National Oceanic and Atmospheric Administration, and the U. S. Geological Survey often point to the main unresolved issues across the science landscape. In the report for 2007–2008 outlining the requirements for the upcoming decade, the committee stressed collecting more observations to help answer climate related questions regarding polar land ice and sea ice as well as ocean characteristics and sea level rise. In seeking out the land and sea ice question, the National Aeronautics and Space Administration established the Ice, Cloud, and Land Elevation Satellite 2 (ICESat-2) mission as the successor to the original ICESat mission (2003–2009; Schutz et al., 2005) with the goal of providing high spatial and temporal coverage of the Earth's polar regions. An overview of the mission requirements and primary scientific goals of ICESat-2 are described in Markus et al. (2017) with an initial overview of performance in Magruder et al. (2019) and Neumann et al. (2019).

While the main objectives for ICESat-2 are related to the land ice elevation and sea ice changes, the satellite collects data over all surface types. ICESat-2 employs a photon counting LiDAR that operates at 532 nm (green in the visible spectrum) with a 10-kHz repetition rate. The Advanced Topographic Laser Altimeter System (ATLAS) uses this high repetition rate combined with the 7-km s^{-1} spacecraft speed to collect photon data along the satellite track every 70 cm with a 12- to 15-m diameter footprint depending on latitude. Three beam pairs are produced by ATLAS, each pair consisting of a strong and weak signal beam. The pairs are separated by 3.3 km in the cross-track direction with separation of 90 m between the strong and weak beams. Each individual photon detected by ATLAS is geolocated using the travel time, orbit position and attitude of the spacecraft. Geolocation and vertical accuracy is determined using trusted data at known ground sites (i.e., Magruder & Brunt, 2018) and to date are performing better than the mission measurement requirements as initially described in Markus et al. (2017).

The signal return rates per laser shot vary between surface type, where highly reflective surfaces such as ice and snow have ~10 returns per shot (Neuenschwander & Pitts, 2019; Smith et al., 2019). Because the open ocean has low reflectance in the visible spectrum (Hartmann, 1994), ocean signal rates are 0–4 per laser shot, similar to land. Neuenschwander and Magruder (2016) initially showed that the 10-kHz laser repetition rate allows for sufficient aggregate of signal to support surface determination, which can be applied to wave characterization. For this reason, an ocean height product is provided among the ICESat-2 along-track product suite for global applications. The relevant output from this product is significant wave height, but the methods used produce output at a variable resolution due to algorithm requirements. To accommodate local characterization and achieve a detailed analysis requires a robust analytical approach, similar to the process used in the land and vegetation product algorithm.

The observing strategy for ICESat-2, especially for ocean scenes, is not designed to provide large area coverage on short, repeated time scales. Like the Jason altimeter missions, it would require combination with other altimeters to obtain a global representation of the ocean characteristics. It is, however, capable of providing detailed regional and localized ocean observations that can improve the understanding of small-scale processes related to air-sea interaction and ocean-sea ice zones, for example. Local to regional-scale processes are vital to understand because of their overall effect on the large scale processes that are already well observed by satellite-based radar altimeters and incorporated into ocean models. It is the authors' primary goal for this study to provide a discourse on determining similar wave and wind characteristics using the new ICESat-2 photon counting LiDAR data. By providing evidence that high-resolution wave characteristics are useful and obtainable from spaceborne LiDAR, the secondary goal is to show the applicability of ICESat-2 for ocean monitoring. With the high along-track resolution, ICESat-2 has the potential to contribute important wave and wind information to the suite of available products. The sections that follow include a description of the data, a methodology for determining wave and wind characteristics, the overall results and validation of the calculated ocean surface structure, and some conclusions regarding the results and analysis.

2. Data

2.1. Ocean Surface Heights From ICESat-2

Each ATLAS data product designated for release begins with an "ATL" prefix, and details on all of the ICESat-2 products are available in their respective theoretical basis documents, which can be obtained from the National Snow & Ice Data Center. The basic input for determining wave characteristics on the ocean surface are derived from ATL03, which contains the individual geolocated photon information. The standard ocean product is ATL12 (Morison et al., 2019) and the land and vegetation product is ATL08. Applying the ATL08 "ground" surface fit to the ocean, it is possible to determine significant wave height and wave length and develop an energy frequency spectrum to separate swell from wind seas. This experimental product is called ATL08-ocean in this study. The North Atlantic region as shown in the main panel of Figure 1 is used for initial analysis. There were 96 long ocean segments used in this test region, which focused on the first week of data collection from 14–20 October 2018. The full list of these data is provided in the supporting information.

2.2. Wave and Wind Validation

Reanalysis output produced by the European Centre for Medium-Range Weather Forecasts provide joint information on wind and wave properties over the ocean. The ERA-5 Reanalysis (Hersbach et al., 2018; Copernicus Climate Change Service (C3S), 2017) 10-m equivalent neutral wind speed and significant wave characteristics were used in the validation effort. These data are output at hourly intervals with the ocean data available in 0.5° spatial resolution and ocean wind speeds at 0.25° resolution. Because ICESat-2 provides surface heights, it was logical to first verify the significant wave heights and wave length. Consequently, the ocean winds calculated for ICESat-2 are significantly dependent on these components. Ocean vector winds are observed from satellites, such as ASCAT, but data overlap within a 3- to 6-hr time window and over the study area limited the availability of coincident data, similarly to the radar altimeter data for wave height. It is also important to understand the limitations and inherent biases in the reanalysis output. Decker et al. (2012) determined that the ERA-Interim reanalysis (Dee et al., 2011) performed the best for wind speed with a bias of ~1.5 m s^{-1} at the 10-m height relative to tower data. Additional latitudinal biases are also possible because of sea surface temperature (SST) gradients and surface currents (Gaube et al., 2015).

2.3. Wave Energy Spectrum

Wave energy and directional spectra are captured at specific locations by various types of buoys or produced in an ocean model. To compare the spectra determined from the ICESat-2 ocean surface signal, three buoys managed by the National Oceanic and Atmospheric Administration's National Data Buoy Center were selected. Each buoy had to be at least 200 km from land with a water depth of at least 3 km to ensure no shallow water effects on the wave spectra. Three buoys chosen include station 41041, 41047, and 46066. These buoys are located in tropical, subtropical, and midlatitude locations, respectively, to provide a variety of ocean scenarios for validation. The main panel in Figure 1 indicates the location of Stations 41041 and 41047, while the third buoy located south of Alaska is not depicted in the overall coverage. The overlapping orbit segments from ICESat-2 that occur within 15 km of the buoy location are used in the validation and are shown in subpanels on the right side of Figure 1. To increase the coverage at each buoy, all orbit segments from 14 October 2018 to 15 January, 2019 within the specified limits are included for analysis. The orbit files are also listed in the supporting information.

3. Methodology

3.1. Determining Wave Characteristics From ICESat-2

The photon elevation data in the ATL03 product are obtained and run through the ATL08 processing algorithm. The ATL03 data include information about the validity of each photon signal and assign a low, medium, or high confidence value. In the land surface calculation, only high confidence values are used, but because the ocean is generally less reflective, medium confidence signal data are included when passed through the ATL08 algorithm. The land surface algorithm uses the Differential, Regressive, and Gaussian Adaptive Nearest Neighbor technique to uniquely determine valid signal in combination with the noise filter provided with the lower level photon data product. A smoothing Savitzky-Golay median filter is then applied along with several iterative filters to determine a "ground" surface. The filtered "ground" line is used to create an initial estimate of the crests and troughs of waves over a 2.5-km segment. Overlapping segments are computed every 0.5 km to ensure consistency in the data. The ground line provides the associated wave lengths of a given segment, and the maximum and minimum surface signal within 17 m of the crest or trough location determined by the ground line provides an estimate of wave amplitude. Figure 2 shows an

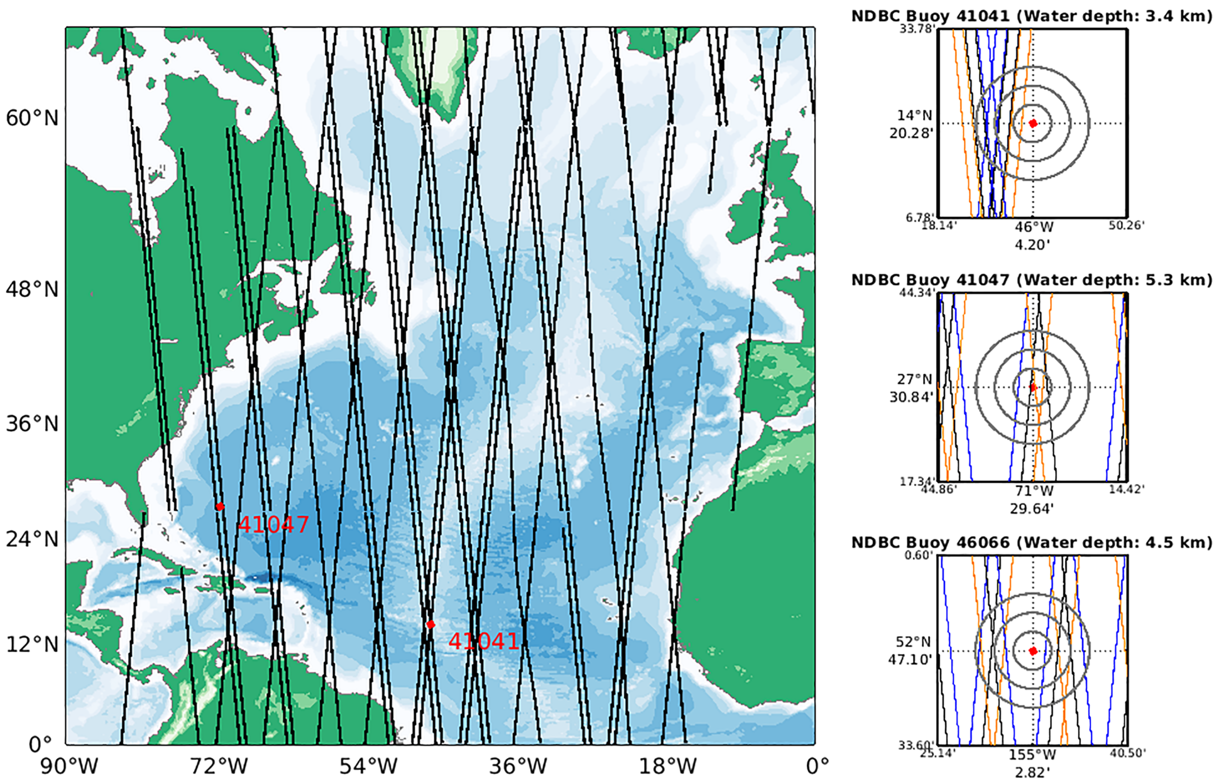

Figure 1. In the main (left) panel, the ICESat-2 orbits used for the North Atlantic region are shown for the period of 14–20 October 2018. Three buoy locations are provided in the right panels, where range rings are given in 5-km intervals. The colors of the tracks indicate which strong beam ground track is used, where Tracks 1–3 are given shown in blue, black, and orange. The underlying map in the left panel shows the water depth across the region, where white regions are less than 600 m in depth.

example over one segment of data from 15 October over the tropical Eastern Atlantic as indicated by the inset map. Highlighted in this figure are the wave features extracted for further calculation. Every 0.1 s in Figure 2 is equivalent to 700-m along track. Given the constraints and dynamic nature of the filtering process, signal photons will be filtered out along the extremes of the ground signal determination, which are shown as gray dots in Figure 2. These points are not background noise that are filtered out by Differential, Regressive, and Gaussian Adaptive Nearest Neighbor.

After determining the wave characteristics from the surface elevation data, calculation of the significant wave height (H_s) and associated wave length (L_s) is completed. Significant wave height is usually interpreted from the wave displacement (i.e., $H_s = 4\times\sqrt{m_0}$, where m_0 is the variance of displacement). This term is nearly identical to the top third of wave heights in a given scene. For ATL08-ocean, H_s is determined by sorting the array of wave heights in descending order and producing a weighted average of the top third of these heights. The weights are based on a confidence flag determined by the ratio of signal photons for an individual wave relative to the expected number of photons per meter. A high weight indicates that enough signal photons are present within the wave to expect confidence in its length and amplitude. It is important to discuss that ICESat-2 orbits will typically not align exactly with the wave direction, and taking the length from the method above would be biased. The solution is to use the ERA-5 wave direction parameter as a guide for determining the wave length. If the direction exceeds 50 degrees rotated from the orbit direction, the data are excluded from initial consideration. For cases that do not exceed this threshold, the angle is taken into account using trigonometric functions to estimate the wave length.

Because each segment contains multiple waves of varying height and length, a wave energy spectrum is produced using a Fourier analysis to help separate swell from wind seas. The frequency is converted to wave length and associated wave period (T) for the spectrum following the typical deep water dispersion relationship ($L = {}^{gT^2}\!/_{2\pi}$), where g is the acceleration due to gravity. Wave spectra often show a double peak with the

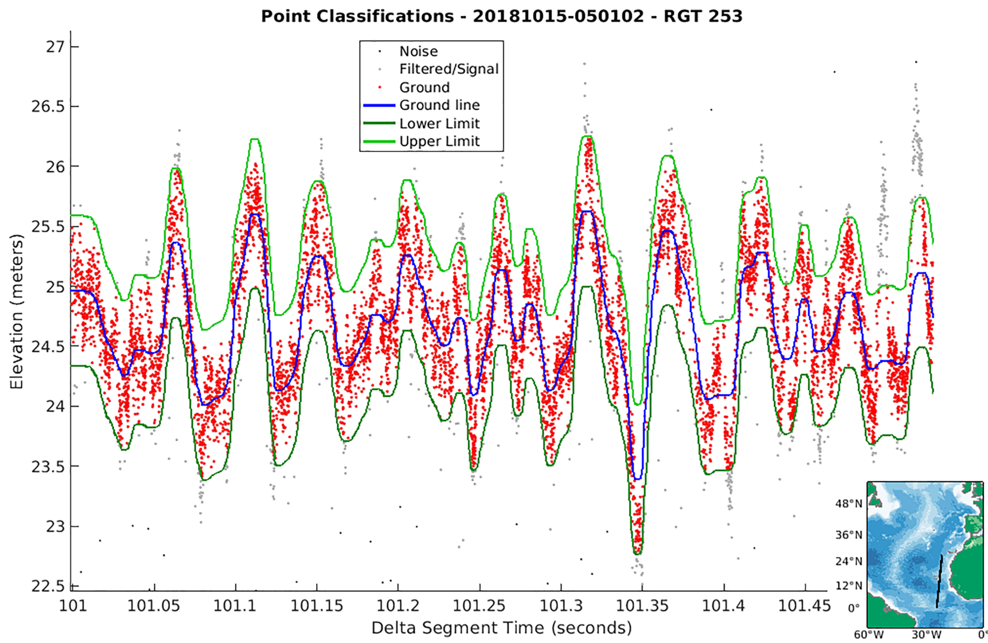

Figure 2. For a portion of the orbit segment from 15 October 2018, the various photon classifications are provided along with the ground line (orange) and the wave envelope (green lines) of the signal. Gray markers indicate filtered noise and signal that do not meet the threshold requirements. The inset panel shows the location of the data.

minimum amplitude between the peaks representing the separation frequency (Aranuvachapun, 1987; Wang & Hwang, 2001). A methodology developed by Earle (1984) empirically derived a way to determine the local wind following the Pierson-Moskowitz spectral model (Pierson & Moskowitz, 1964), but Wang and Hwang (2001) suggest a more direct approach that relates the separation frequency to wind speed. Their equation (9) is given as $f_s = {}^{g}/_{2\pi U}$, where U is the local wind speed. This is one method by which we can determine the local wind speed, but those authors state it has some inconsistencies based on variability in the wave spectra representation and determination of the separation frequency. Because this study directly obtains significant wave height and length, there is an alternative method for computing wind speed and associated drag parameters. Following Taylor and Yelland (2001) and Drennan et al. (2005), the roughness length, z_0, can be calculated directly from the significant wave height and peak wavelength through the following equation:

$$z_0 = H_s\left[1200\times\left(\frac{H_s}{L_s}\right)^{4.5}\right]. \tag{1}$$

Wind speed at a particular height above a surface is calculated using the traditional Monin-Obukhov similarity theory based logarithmic function:

$$U(z) = \frac{u_*}{k}\ln\left(\frac{z}{z_0}\right), \tag{2}$$

where u_* is the friction velocity, k is the von Kármán constant, and z is the standard ocean wind measurement height of 10 m (U_{10}). Drennan et al. (1999) indicates that the similarity theory was originally determined for land but applied to ocean conditions. With the changing state of the waves, similarity theory is not applicable close to the surface as momentum between the air and sea is directly transferred and is also impacted by long wave swell (Donelan et al., 1997). Away from the surface, it tends to hold up better and is useful for evaluating wind seas. To calculate the friction velocity at the standard wind speed height, the modified equation from Drennan et al. (2003) is used:

$$u_* = c_p \left(\frac{z_0}{3.35 \times H_s} \right)^{0.294}. \tag{3}$$

In equation (3), the dispersion relationship is given by $c_p = \sqrt{gL_s/_{2\pi}}$. The drag coefficient ($C_D$) can also be calculated with the given variables using $C_D = {}^{k}/_{\ln(z/z_0)}$. For every designated segment that meets the criteria for computing wind and wave features, the significant wave height and length, wave period, 10-m wind speed and drag coefficient, and wave energy spectra are computed. These are produced for each of the strong beams at a spacing of 0.5 km for overlapping 2.5-km segments. The equations above reflect neutral boundary layer conditions, which will not be appropriate in every scenario (i.e., Kara et al., 2008). An analysis of the lower boundary layer profile in the reanalysis output indicates that a majority of the ICESat-2 calculated winds are within a neutral to slightly unstable profile. Most satellite-based wind estimates are validated with equivalent neutral winds, and the ICESat-2 determined wind speeds also use this value for validation to help account for differences due to the boundary layer stability. More details on potential biases are provided in the supporting information.

3.2. Significant Wave, Wind, and Wave Spectra Validation

For the data collected over the North Atlantic region, ERA-5 reanalysis data are matched to the closest time of the ICESat-2 orbit section. The ICESat-2 data can essentially be treated as a snapshot of ocean characteristics because of the satellite flight speed. The position of the ATL08-ocean products is then used to perform a bilinear interpolation of the ERA-5 data with an inverse distance weighting scheme applied to the interpolation. The resulting values for significant wave height, wave length, and wind speed are then coincident to the same variables in the ATL08-ocean data. This process is completed for all the orbit segments where a valid ocean product was created. A quality check is performed during the ATL08-ocean processing for representativeness of the wave features for deep water waves, eliminating contamination from shallow water coastal zones.

Energy spectra are determined differently by the buoys than by ATL08-ocean because of the observation strategy. For the buoy data, significant wave heights are computed over a 10- to 20-min period, and although it is not expressly stated, the wave spectra are computed from this time series of waves. Assuming a typical deep water wave speed based on the dispersion relationship mentioned in the previous section, swell would propagate through the buoy location from a distance of approximately 15 km away. Wave spectra calculated from ICESat-2 from the 15 km threshold mentioned in section 2.3 would have observed similar conditions experienced by the buoy. Therefore, the buoy and the satellite effectively observe the same ocean conditions. Data from each strong beam are also distance weighted with their proximity to the buoy to provide more accurate statistics. From the energy spectra of each data source, the peak swell and wind wave frequency are determined and statistically evaluated.

4. Initial Results and Validation

4.1. Wave and Wind Characteristics and Validation

Based on the selected set of orbits over the North Atlantic, the median H_s is 2.02 m with 90% of heights between 1.34 and 3.22 m. For the ERA-5 interpolated H_s, the results are similar to ICESat-2. Median and inner 90% of the distribution are 1.90 m and between 1.32 and 4.78 m, respectively. For the wave length data determined by the ICESat-2 method, the median is 357.3 m, and the inner 90% fall between 268.7 and 517.1 m. The corresponding values for ERA-5 are 364.6 m and 278.3 to 523.7 m, respectively. The U_{10} data have somewhat more variability than the wave results with a median value of 5.9 m s^{-1} and 90% of the data between 3.3 and 9.4 m s^{-1}. The equivalent neutral wind speeds provided by the ERA-5 data set seem to coincide with those determined by the satellite as the median and inner 90% are 6.6 m s^{-1} and between 3.2 and 10.8 m s^{-1}, respectively. These comparisons indicate that it is possible to obtain wind speeds, wave height, and wave length estimates that are within the expected value given in the validation data. A paired Kolmogorov-Smirnov test on the cumulative distribution of H_s, L_s, and U_{10} indicate that the distributions are not significantly different at the 99.9% confidence level.

Establishing that the wave height, wave length, and 10-m winds derived from the ICESat-2 adequately resemble the same features from an independent validation source is encouraging to see, but it is also

10.1029/2019GL085907

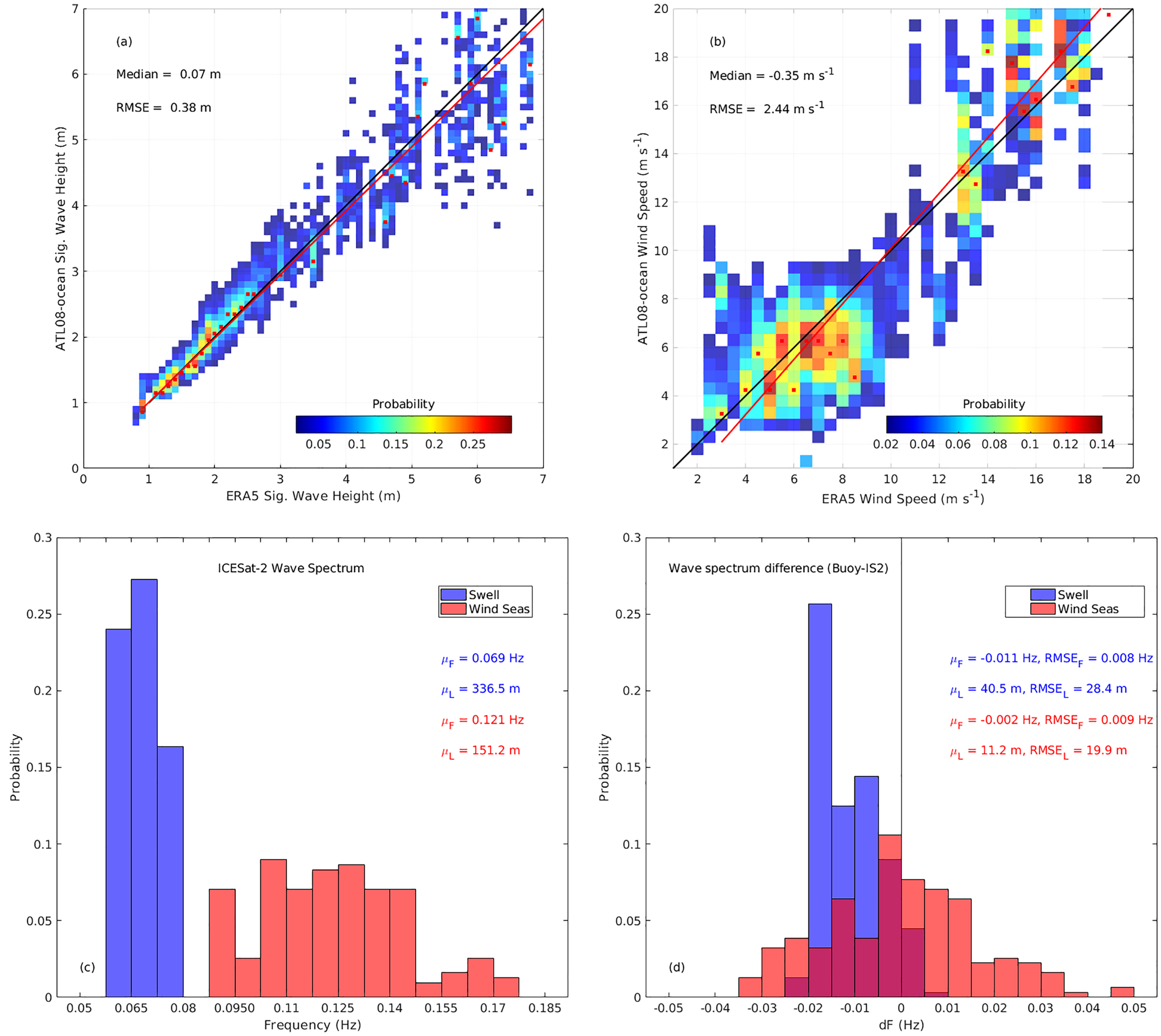

Figure 3. Joint probability histograms for significant wave height (a) and 10-m wind speed (b) are provided for ICESat-2 and ERA-5 reanalysis pairs. The ERA-5 data in (b) are equivalent neutral wind speeds. The black line is the 1:1 relationship line, and the red line indicates the maximum probability for a particular ERA-5 bin. Histograms of ICESat-2 peak frequency of the swell and wind seas determined from the wave energy spectrum are shown in (c). In (d), histograms of the peak frequency differences are provided. The two length scales listed on the top axis of (d) are because of nonlinear transformation of frequency and length.

important to determine if the point by point comparisons match well. The focus of this section will be on significant wave height and wind speed because of the more direct comparison with the ERA-5 reanalysis. Discussion of the wave length statistics is provided in the supporting information. Joint probability histograms are shown for each parameter in Figures 3a and 3b for the cases that meet the wave direction criteria. For significant wave height, the ICESat-2 values are biased slightly high with a mean difference of 0.07 m and standard deviation of 0.35 m. These statistics are within the constraints of other altimeters, indicating that the wave heights perform comparably well to other observations but at a higher horizontal resolution. The wind speed performance is not as robust as the wave heights, but the highest probability of likely wind speed matches closely with the ERA-5 winds. The mean difference is -0.26 m s^{-1}, and the standard deviation of 2.2 m s^{-1} is similar to the standard deviation and root-mean-square error of wind estimates from other satellites, which are typically in the range of 1.6–2.0 m s^{-1} when compared to numerical models (Cavaleri et al., 2019; Verhoef et al., 2017). There are still some instances where the winds are above this threshold, but overall, the performance provides confidence in obtaining ocean winds from ICESat-2. For reference, the deviations for other wind satellites are closer to ~1.0 m s^{-1} when compared to buoy observations (Stefellen et al., 2017; Wentz et al., 2017). More details on related deviations are provided in the supporting information text.

4.2. Wave Spectra Validation

Buoys are suited for obtaining time series changes in ocean waves and can easily provide wave energy spectra for interpreting swell and wind wave amplitude and direction. Even though the data collected by ICESat-2 are not a typical time series, the Fourier analysis computed over the 2.5 km segment can almost be treated as one, where the center segment location would represent a buoy location. Waves in the scene have either been experienced at that point or will be experienced after data collection, depending on the predominant wave direction. To evaluate the wave spectra determined by the satellite, the primary and secondary amplitude peaks indicate the swell and wind sea frequencies. The differences between these two peaks for both data sources are compared for the three buoy locations. Data from multiple ICESat-2 orbits are not compared to the same buoy observation to maintain statistical integrity. Figure 3c shows the ICESat-2 histograms for the peak swell and wind wave frequencies with clear separation between the two signals. The mean frequency for swell is 0.069 Hz, which translates to ~340-m wave length. The uncertainty in the peak swell frequency is 8%. For wind waves, the mean frequency is 0.121 Hz or ~150-m wave length with an uncertainty of 11%. The wave generation mechanism for these two types of waves is apparent in the distribution of peaks, where more uncertainty is present in the wind generated waves.

Figure 3d shows the difference of the ICESat-2 and buoy peak frequencies with negative values indicating a high bias in the ICESat-2 wave spectra. A bias of −0.011 Hz (~46 m) is present in the swell signal with a standard deviation of 0.006 Hz. This variation in the difference indicates a ±7.8% change relative to the mean peak swell frequency from the buoy. The mean bias for the wind wave component is close to 0, and similarly to the peak swell frequency, the standard deviation indicates a ±12.9% change relative to the peak wind wave frequency. The slightly increased variability in the wind wave peak frequency relative to the buoy could be an effect of multiple factors. It is possible that wind speed differences across the 30 km diameter circle around the buoy are variable enough to produce different wave features. There could also be variations in the calculation of the peak frequency based on the photon wave determination. Regardless of the reason for the higher wind wave uncertainty, the wave spectra from ICESat-2 compare well to buoy spectra and indicate a way to represent detailed wave components from satellite data.

5. Conclusions and Future Work

The new ICESat-2 spaced-based LiDAR system is an important tool for studying the Earth's cryosphere, especially with recent reports indicating drastic changes in the polar ice sheets and sea-ice coverage. However, ICESat-2 is not limited to the poles as companion atmospheric, oceanic, and terrestrial observations are also obtained. Ocean observations at the global scale are only realistically collected by satellites, but the current altimetry missions and even the standard ICESat-2 ocean product do not fully promote the wave features that are observed in the ICESat-2 photon data. The sophistication of the terrain surface finding strategy provides a way to enhance these details, and this study uses the same methodology for finding the variation of the ocean surface heights to the point where individual waves are observed from space. High-resolution wave and wind characteristics are presented and indicate good agreement with independent data sources. Wave spectra are more variable in their uncertainty but also show promise for future use in physical oceanography studies. The results indicate that ocean wave characteristics determined through the adapted ATL08 surface finding methodology are accurate and improve the ability to study the ocean at higher resolutions with relatively high confidence.

The main goal of this study was to show the capability of the observations in open ocean scenes. The authors also plan to further investigate how these measurements might provide additional improvements to coastal altimetry where standard radar altimeters are unable to obtain reliable observations. Given the results of this study provide analysis for deep water only, some modifications related to the use of dispersion equations would be necessary. Accounting for boundary layer stability will continue to be considered too. Because sea levels are already beginning to rise (Merrifield et al., 2009; Nerem et al., 2018) and coastal changes vary between locations (Melet et al., 2018) due to wave patterns and tidal influence, it is important to gain a better sense of the changes in coastal locations across the globe. There is also potential to use this technique to study the interaction over the atmosphere-ocean-sea ice interface in the Arctic. There are many questions that remain unanswered simply due to lack of extensive observations. Expansion and adaptation of the methodology used in this study could help answer some of those questions and connect changes in ocean conditions to changes in sea ice coverage or thickness. These ideas are certainly not exhaustive of the future studies to perform using ICESat-2 data but are two prominent issues that can be addressed in more detail during the ICESat-2 era.

Acknowledgments
The authors wish to thank the NASA ICESat-2 science team for their hard work preparing the data used in this study. We would also like to acknowledge Katherine Pitts for her significant contributions to the ATL08 algorithm and code. Two anonymous reviewers also aided in clarification of certain topics discussed in the paper. There are no real or perceived conflicts of interest for the lead author or coauthors. The ICESat-2 data are available through the National Snow & Ice Data Center (NSIDC). The geolocated photon data are found online (https://nsidc.org/data/ATL03/versions/2). Funding for the lead author was provided by internal support at Applied Research Laboratories and for the coauthors through ICESat-2 science team support.

References

Aranuvachapun, S. (1987). Parameters of JONSWAP spectral model for surface gravity waves-II. Predictability from real data. *Journal of Oceanic Engineering*, *14*, 101–115. https://doi.org/10.1016/0029-8018(87)90072-2

Benveniste, J. (2011). Radar altimetry: Past, present, and future. In S. Vignudelli, A. Kostianoy, P. Cipollini, & J. Benveniste (Eds.), *Coastal altimetry* (pp. 1–17). Berlin, Germany: Springer. https://doi.org/10.1007/978-3-642-12796-0_1

Bourassa, M. A., Meissner, T., Cerovecki, I., Chang, P. S., Dong, X., de Chiara, G., et al. (2019). Remotely sensed winds and wind stresses for marine forecasting and ocean modeling. *Frontiers in Marine Science*, *6*, 1–28. https://doi.org/10.3389/fmars.2019.00443

Cavaleri, L., Bertotti, L., & Pezzutto, P. (2019). Accuracy of altimeter data in inner and coastal seas. *Ocean Science*, *15*, 227–233. https://doi.org/10.5194/os-15-227-2019

Copernicus Climate Change Service (C3S) (2017). ERA5: Fifth generation of ECMWF atmospheric reanalyses of the global climate. Copernicus Climate Change Service Climate Data Store (CDS), 01 December 2018. https://cds.climate.copernicus.eu/cdsapp#!/home

Decker, M., Brunke, M. A., Wang, Z., Sakaguchi, K., Zeng, X., & Bosilovich, M. G. (2012). Evaluation of reanalysis products from GSFC, NCEP, and ECMWF using flux tower observations. *Journal of Climate*, *25*, 1916–1944. https://doi.org/10.1175/JCLI-D-11-00004.1

Dee, D. P., Uppala, S. M., Simmons, A. J., Berrisford, P., Poli, P., Kobayashi, S., et al. (2011). The ERA-Interim reanalysis: Configuration and performance of the data assimilation system. *Quarterly Journal of the Royal Meteorological Society*, *137*(656), 553–597. https://doi.org/10.1002/qj.828

Desai, S. (2016). Jason-3 GPS based orbit and SSHA OGDR. Ver. A., PO.DAAC, CA, USA.

Donelan, M. A., Drennan, W. M., & Katsaros, K. B. (1997). The air-sea momentum flux in conditions of wind sea and swell. *Journal of Physical Oceanography*, *27*, 2087–2099. https://doi.org/10.1175/1520-0485(1997)027<2087:TASMFI>2.0.CO;2

Drennan, W. M., Graber, H. C., Hauser, D., & Quentin, C. (2003). On the wave age dependence of wind stress over pure wind seas. *Journal of Geophysical Research*, *108*(C3), 8062. https://doi.org/10.1029/2000JC000715

Drennan, W. M., Kahma, K. K., & Donelan, M. A. (1999). On momentum flux and velocity spectra over waves. *Boundary-Layer Meteorology*, *92*, 489–515. https://doi.org/10.1023/A:1002054820455

Drennan, W. M., Taylor, P. K., & Yelland, M. J. (2005). Parameterizing the sea surface roughness. *Journal of Physical Oceanography*, *35*, 835–848. https://doi.org/10.1175/JPO2704.1

Earle, M. D. (1984). Development of algorithms for separation of sea and swell, National Data Buoy Center Tech. Rep. MEC-87-1, 53 pp.

Figa-Saldaña, J., Wilson, J. J. W., Attema, E., Gelsthorpe, R., Drinkwater, M. R., & Stoffelen, A. (2002). The advanced scatterometer (ASCAT) on the meteorological operational (MetOp) platform: A follow on for European wind scatterometers. *Canadian Journal of Remote Sensing*, *28*(3), 404–412. https://doi.org/10.5589/m02-035

Gaube, P., Chelton, D. B., Samelson, R. M., Schlax, M. G., & O'Neill, L. W. (2015). Satellite observations of mesoscale eddy-induced Ekman pumping. *Journal of Physical Oceanography*, *45*, 104–132. https://doi.org/10.1175/PO-D-14-0032.1

Hartmann, D. L. (1994). *Global physical climatology*. San Diego, CA: Academic Press.

Hersbach, H., de Rosnay, P., Bell, B., Schepers, D., Simmons, A., Soci, C., et al. (2018). Operational global reanalysis: Progress, future directions and synergies with NWP, ERA Report Series, 27, 1-65. doi: 10.21957/tkic6g3wm.

Kara, A. B., Wallcraft, A. J., & Bourassa, M. A. (2008). Air-sea stability effects on the 10 m winds over the global ocean: Evaluations of air-sea flux algorithms. *Journal of Geophysical Research*, *113*, C04009. https://doi.org/10.1029/2007JC004324

Lambin, J., Morrow, R., Fu, L. L., Willis, J. K., Bonekamp, H., Lillibridge, J., et al. (2010). The OSTM/Jason-2 mission. *Marine Geodysy*, *33* (sup1), 4–25. https://doi.org/10.1080/01490419.2010.491030

Magruder, L., Neumann, T., Fricker, H., Farrell, S., Brunt, K., Gardner, A., et al. (2019). New Earth orbiter provides a sharper look at a changing planet. *Eos*, *100*. https://doi.org/10.1029/2019EO133233

Magruder, L. A., & Brunt, K. M. (2018). Performance analysis of airborne photon-counting lidar data in preparation for the ICESat-2 mission. *IEEE Transactions on Geoscience and Remote Sensing*, *56*, 2911–2918. https://doi.org/10.1109/TGRS.2017.2786659

Markus, T., Neumann, T., Martino, A., Abdalati, W., Brunt, K., Csatho, B., et al. (2017). The Ice, Cloud, and land Elevation Satellite-2 (ICESat-2): Science requirements, concept, and implementation. *Remote Sensing of Environment*, *190*, 260–273. https://doi.org/10.1016/j.rse.2016.12.029

Mears, C. A., Smith, D. K., & Wentz, F. (2015). Estimated errors in retrievals of ocean parameters from SSMIS. *Journal of Geophysical Research: Atmospheres*, *120*, 5816–5830. https://doi.org/10.1002/2014JD023049

Melet, A., Meyssignac, B., Almar, R., & Le Cozannet, G. (2018). Under-estimated wave contribution to coastal sea-level rise. *Nature Climate*, *8*, 234–239. https://doi.org/10.1038/s41558-018-0088-y

Merrifield, M. A., Merrifield, S. T., & Mitchum, G. T. (2009). An anomalous recent acceleration of global sea level rise. *Journal of Climate*, *22*, 5772–5781. https://doi.org/10.1175/2009JCLI2985.1

Morison, J. H., Hancock, D., Dickinson, S., Robbins, J., Roberts, L., Kwok, R., et al. (2019). Algorithm Theoretical Basis Document (ATBD) for ocean surface height (ATL12). ICESat-2 Scientific Computing Facility. https://icesat-2-scf.gsfc.nasa.gov/atbd_docs

Nerem, R. S., Beckley, B. D., Fasullo, J. T., Hamlington, B. D., Masters, D., & Mitchum, G. T. (2018). Climate-change-driven accelerated sea-level rise detected in the altimeter era. *Proceedings of the National Academy of Sciences*, *115*(9), 2022–2025. https://doi.org/10.1073/pnas.1717312115

Neuenschwander, A., & Pitts, K. (2019). The ATL08 land and vegetation product for the ICESat-2 mission. *Remote Sensing of Environment*, *221*, 247–259. https://doi.org/10.1016/j.rse.2018.11.005

Neuenschwander, A. L., & Magruder, L. A. (2016). The potential impact of vertical sampling uncertainty on ICESat-2/ATLAS terrain and canopy height retrievals for multiple ecosystems. *Remote Sensing*, *8*(12), 1039. https://doi.org/10.3390/rs8121039

Neumann, T. A., Martino, A. J., Markus, T., Bae, S., Bock, M. R., Brenner, A. C., et al. (2019). The Ice, Cloud, and Land Elevation Satellite-2 mission: A global geolocated photon product derived from the Advanced Topographic Laser Altimeter System. *Remote Sensing of Environment*, *233*, 111325. https://doi.org/10.1016/j.rse.2019.111325

Pierson, W. J., & Moskowitz, L. (1964). A proposed spectral form for fully developed wind seas based on the similarity theory of S. A. Kitaigorodskii. *Journal of Geophysical Research*, *69*, 5181–5190. https://doi.org/10.1029/JZ069i024p05181

Schultz-Stellenfleth, J., König, T., & Lehner, S. (2007). An empirical approach for the retrieval of integral ocean wave parameters from synthetic aperture radar data. *Journal of Geophysical Research*, *112*, C03019. https://doi.org/10.1029/2006JC003970

Schutz, B. E., Zwally, H. J., Shuman, C. A., Hancock, D., & DiMarzio, J. P. (2005). Overview of the ICESat mission. *Geophysical Research Letters*, *32*, L21S01. https://doi.org/10.1029/2005GL024009

Smith, B., Fricker, H. A., Holschuh, N., Gardner, A. S., Adusumilli, S., Brunt, K. M., et al. (2019). Land ice height-retrieval algorithm for NASA's ICESat-2 photon-counting laser altimeter. *Remote Sensing of Environment*, *233*, 111352. https://doi.org/10.1016/j.rse.2019.111352

Stefellen, A., Verspeek, J. A., Vogelzang, J., & Verhoef, A. (2017). The CMOD7 geophysical model function for ASCAT and ERS wind retrievals. *IEEE J Selected Topics in Applied Earth Observations and Remote Sensing*, *10*, 2123–2134. https://doi.org/10.1109/JSTARS.2017.2681806

Taylor, P. K., & Yelland, M. J. (2001). The dependence of sea surface roughness on the height and steepness of waves. *Journal of Physical Oceanography*, *31*, 572–590. https://doi.org/10.1175/1520-0485(2001)031<0572:TDOSSR>2.0.CO;2

Verhoef, A., Vogelzang, J., Verspeek, J., & Stoffelen, A. (2017). Long-term scatterometer wind climate data records. *IEEE Journal of Selected Topics in Applied Earth Observations and Remote Sensing*, *10*, 2186–2194. https://doi.org/10.1109/JSTARS.2016.2615873

Wang, D. W., & Hwang, P. A. (2001). An operational method for separating wind sea and swell from ocean wave spectra. *Journal of Atmospheric and Oceanic Technology*, *18*, 2052–2062. https://doi.org/10.1175/1520-0426(2001)018<2052:AOMFSW>2.0.CO;2

Wentz, F., Ricciardulli, L., Rodriguez, E., Stiles, B. W., Bourassa, M. A., Long, D. G., et al. (2017). Evaluating and extending the ocean winds data climate record. *J. Selected Topics in Applied Earth Observations and Remote Sensing*, *10*(5), 2165–2185. https://doi.org/10.1109/JSTARS.2016.2643641

Reference From the Supporting Information

Stull, R. B. (1988). *An introduction to boundary layer meteorology*. Boston, MA: Kluwer Academic Publishers.